

A THIRTY KILOPARSEC CHAIN OF “BEADS ON A STRING” STAR FORMATION BETWEEN TWO MERGING EARLY TYPE GALAXIES IN THE CORE OF A STRONG-LENSING GALAXY CLUSTER

GRANT R. TREMBLAY¹, MICHAEL D. GLADDERS², STEFI A. BAUM³, CHRISTOPHER P. O’DEA³, MATTHEW B. BAYLISS^{4,5},
KEVIN C. COOKE³, HÅKON DAHLE⁶, TIMOTHY A. DAVIS¹, MICHAEL FLORIAN², JANE R. RIGBY⁷,
KEREN SHARON⁸, EMMARIS SOTO⁹, AND EVA WUYTS¹⁰

Accepted for Publication in *ApJ Letters*, 24 June 2014

ABSTRACT

New *Hubble Space Telescope* (*HST*) ultraviolet and optical imaging of the strong-lensing galaxy cluster SDSS J1531+3414 ($z = 0.335$) reveals two centrally dominant elliptical galaxies participating in an ongoing major merger. The interaction is at least somewhat rich in cool gas, as the merger is associated with a complex network of nineteen massive superclusters of young stars (or small tidal dwarf galaxies) separated by ~ 1 kpc in projection from one another, combining to an estimated total star formation rate of $\sim 5 M_{\odot} \text{ yr}^{-1}$. The resolved young stellar superclusters are threaded by narrow $\text{H}\alpha$, $[\text{O II}]$, and blue excess filaments arranged in a network spanning ~ 27 kpc across the two merging galaxies. This morphology is strongly reminiscent of the well-known “beads on a string” mode of star formation observed on kpc-scales in the arms of spiral galaxies, resonance rings, and in tidal tails between interacting galaxies. Nevertheless, the arrangement of this star formation relative to the nuclei of the two galaxies is difficult to interpret in a dynamical sense, as no known “beads on a string” systems associated with kpc-scale tidal interactions exhibit such lopsided morphology relative to the merger participants. In this Letter we present the images and follow-up spectroscopy, and discuss possible physical interpretations for the unique arrangement of the young stellar clusters. While we suggest that this morphology is likely to be dynamically short-lived, a more quantitative understanding awaits necessary multiwavelength follow-up, including optical integral field spectroscopy, ALMA sub-mm interferometry, and *Chandra* X-ray imaging.

Subject headings: galaxies: clusters: general — gravitational lensing: strong — galaxies: interactions — galaxies: star formation — galaxies: clusters: individual (SDSS J1531+3414)

1. INTRODUCTION

SDSS J1531+3414 is a strong lensing cluster of galaxies at redshift $z = 0.335$ (e.g., Hennawi et al. 2008; Oguri et al. 2009, 2012; Gralla et al. 2011; Bayliss et al. 2011; Postman et al. 2012). Ground-based imaging of the cluster center reveals high surface brightness gravitational arcs from at least two lensed background galaxies at $z \approx 1.1$ and $z \approx 1.3$ (Hennawi et al. 2008; Bayliss et al. 2011), enabling weak- and strong-lensing analysis that yields a cluster mass of $M_{200} = 5.13^{+1.33}_{-1.19} \times 10^{14} h^{-1} M_{\odot}$ (Oguri et al. 2012). The cluster core was recently imaged as part of strong lensing imaging program with the *Hubble Space Telescope* (*HST*). These new

high spatial resolution images reveal that the two giant elliptical galaxies in the cluster core are likely in the process of merging. Most remarkably, the merger is associated with ongoing or very recent star formation arranged in a ~ 27 kpc-scale network of young stellar superclusters separated ~ 1 kpc in projection from one another along faint and narrow filaments, resembling a broken pearl necklace. While indeed strongly reminiscent of the well-known “beads on a string” mode of star formation frequently observed in the arms of spiral galaxies, resonance rings, and tidal arms that bridge interacting galaxies (e.g., Elmegreen & Efremov 1996), the morphology and orientation of this particular chain is unlike any known merging system, and the phenomenon is rarely (if ever) observed in giant early type galaxies (e.g., Kaviraj et al. 2012).

In this Letter we present the new *HST* images of the merging elliptical galaxies and the associated network of young stellar superclusters. Details of the observations are given in Table 1 and §2, and the results presented in §3 are discussed in §4. Throughout this Letter we assume $H_0 = 71 \text{ km s}^{-1} \text{ Mpc}^{-1}$, $\Omega_M = 0.27$, and $\Omega_{\Lambda} = 0.73$. In this cosmology, $1''$ corresponds to 4.773 kpc at the redshift of the two merging ellipticals in the cluster center ($z = 0.335$), where the associated luminosity and angular size distances are 984.4 and 1756.1 Mpc, respectively, and the age of the Universe is 9.954 Gyr.

2. OBSERVATIONS

Initially intended to study the higher redshift background galaxies gravitationally lensed by the cluster, *HST* imaging of SDSS J1531+3414 was obtained in Cycle 20 (GO program 13003, PI: Gladders) with the Wide Field Camera 3 (WFC3, Dressel 2012). The target was observed with four broadband

arXiv:1407.2251v1 [astro-ph.GA] 8 Jul 2014

¹ European Southern Observatory, Karl-Schwarzschild-Str. 2, 85748 Garching bei München, Germany; grant.tremblay@eso.org

² Department of Astronomy & Astrophysics and Kavli Institute for Cosmological Physics, University of Chicago, 5640 S. Ellis Ave., Chicago, IL 60637, USA

³ Chester F. Carlson Center for Imaging Science and School of Physics and Astronomy, Rochester Institute of Technology, 84 Lomb Memorial Drive, Rochester, NY 14623, USA

⁴ Department of Physics, Harvard University, 17 Oxford St., Cambridge, MA 02138, USA

⁵ Harvard-Smithsonian Center for Astrophysics, 60 Garden Street, Cambridge, MA 02138, USA

⁶ Institute of Theoretical Astrophysics, University of Oslo, P.O. Box 1029, Blindern, N-0315 Oslo, Norway

⁷ Observational Cosmology Laboratory, NASA Goddard Space Flight Center, Code 665, Greenbelt, MD 20771 USA

⁸ Department of Astronomy, University of Michigan, 500 Church Street, Ann Arbor, MI 48109, USA

⁹ Department of Physics, The Catholic University of America, 200 Hanan Hall, Washington, DC 20064, USA

¹⁰ Max-Planck-Institut für Extraterrestrische Physik, Postfach 1312, Giessenbachstr., 85741 Garching bei München, Germany

TABLE 1
 SUMMARY OF OBSERVATIONS

Observatory	Instrument	Filter / Config.	Waveband / Central λ / Line	Integration Time	Obs. Date	Comment
<i>HST</i>	WFC3 / UVIS	F390W	Rest Frame NUV / 3923 Å	2256 sec	6 May 2013	Young stellar component
...	...	F606W	Blue optical / 5887 Å	1440 sec	...	Includes [O II], H β
...	...	F814W	Optical / 8026 Å	1964 sec	...	Includes H α +[N II]
...	WFC3 / IR	F160W	Red optical / 1.537 μ m	912 sec	...	Old stellar component
FOLLOW-UP OBSERVATIONS						
NOT	ALFOSC	Grism #7 / 1''	5260 Å / [O II], Ca II H&K	2400 sec	29 Apr 2014	Redshift confirmation
...	...	Grism #5 / 2''5	7000 Å / H α + [N II]
IRAM 30-meter	EMIR	...	86 GHz / Rest frame CO(1–0)	2880 sec	22 Dec 2013	Non-detection

filters over three *HST* orbits, resulting in broad and essentially gap-free coverage over the near-ultraviolet (NUV) and optical wavelength range. This Letter also presents follow-up Nordic Optical Telescope (NOT) slit spectroscopy and a short IRAM 30-meter CO(1–0) observation. More information regarding all new data presented in this paper can be found in Table 1.

The *HST* products were calibrated and reduced using the on-the-fly recalibration pipeline and the ASTRODRIZZLE / DRIZZLEPAC packages provided by the Space Telescope Science Institute (Fruchter et al. 2010). Images were drizzled to the same 0.''03 pixel frame using a 0.8 “pixfrac” Gaussian kernel. An RGB “pretty picture” composite combining all four filters was made using the TRILOGY code¹¹ kindly provided by Dan Coe (see §2 of Coe et al. 2012) and the CLASH team (Postman et al. 2012). More details pertaining to reduction of the *HST* data can be found in Bayliss et al. (2013).

3. RESULTS

3.1. The merging elliptical galaxies

We present the new *HST* data as an RGB composite in Fig. 1. The images used in this composite are shown individually in Fig. 2, which uses contours and labels to highlight various features of interest. As is evident from these Figures, the cluster center harbors two elliptical galaxies whose nuclei are separated ~ 7 kpc (1.''5) in projection from one another. The combined projected stellar envelope of both galaxies extends ~ 100 kpc ($\sim 22''$) across the major axis of the lowest surface brightness isophote, though their light is very centrally concentrated with an *r*-band Petrosian radius of ~ 30 kpc ($\sim 7''$). Both new and archival optical spectroscopy confirms that this is no mere projection effect — the galaxies indeed share a common redshift, such that their stellar halos must be deeply embedded in one another over at least ~ 20 kpc scales.

This is evident in archival Sloan Digital Sky Survey (SDSS, York et al. 2000) optical spectroscopy, which we present in the leftmost panels of Fig. 3. While the SDSS spectrum is from a fiber that covers the nuclei of both galaxies (see top left panel of Fig. 3), it features a singular line system including Mg, Na D, and Ca II H+K absorption tracing the old stellar component, all at a common redshift of $z = 0.3350 \pm 0.0002$ (consistent with the SDSS photometric redshift). This serves as strong evidence that the galaxies are indeed merging, as they would have been bright enough to manifest as two distinct-redshift line systems if indeed they were two otherwise unrelated objects seen in projection.

The merger hypothesis is confirmed by follow-up slit spectroscopy (see Table 1) obtained with the ALFOSC spectrograph on the Nordic Optical Telescope (NOT), the results of

which are presented in the rightmost panels of Fig. 3. As is evident from the [O II] and Ca II lines extracted from the southeastern (SE) and northwestern (NW) galaxy nuclei (see bottom-right panel), the maximum spectroscopically permissible velocity offset between the galaxies is ~ 280 – 300 km sec^{-1} , far too small for these to be unrelated galaxies in the Hubble flow. Any 3D configuration consistent with spectral constraints results in their stellar envelopes being deeply embedded in one another over ~ 20 kpc scales. We therefore conclude that the two ellipticals (which are of roughly equal stellar mass, sharing similar surface brightnesses) are undergoing a major merger.

As noted above, the cluster mass derived from strong+weak lensing analysis is $5.13^{+1.33}_{-1.19} \times 10^{14} h^{-1} M_{\odot}$ (Oguri et al. 2012). The implied projected 1D velocity dispersion from such a mass would be of order ~ 750 km sec^{-1} , consistent with the measured velocity dispersion from 11 member galaxies of 998^{+120}_{-194} km sec^{-1} (Bayliss et al. 2011). The expectation value for pairwise velocities along the line of sight would therefore be $\gtrsim 1000$ km sec^{-1} , rather more than the ~ 280 km sec^{-1} permitted by our follow-up spectroscopy. The NOT data therefore suggest that the trajectories of the merger participants lie mostly in the plane of the sky. While the galaxy stellar isophotes are mostly smooth, unsharp masks and a F606W/F160W color map reveal residual surface brightness fluctuations between and around both nuclei, suggestive of some dynamical disturbance in the old stellar component as a result of the merger.

3.2. The young super star clusters

Far more dramatic than the merging galaxies is the F390W image of rest-frame NUV continuum emission mostly arising from young ($\lesssim 300$ Myr), massive ($\gtrsim 5 M_{\odot}$) stars. This is seen in blue on the rightmost panel of Fig. 1, and shown in the bottom-left panel of Fig. 2. The NUV continuum emission is shown in green contours on the F160W image in the top-left panel of Fig. 2. Not counting the nuclei of the two elliptical galaxies, the emission consists of at least 19 stellar superclusters (or perhaps tidal dwarf galaxies) ~ 0.5 – 1 kpc in diameter. The 19 stellar clusters are enhanced in NUV surface brightness by factors of 2–10 over the filaments in which they are embedded. Each of these superclusters are numerically labeled in the bottom-right panel of Fig. 2, which shows an unsharp mask revealing residual [O II] and blue excess emission in the F606W image.

The young stellar superclusters are roughly equally spaced along 3–4 narrow (1–2 kpc wide), straight filaments roughly ~ 10 kpc in projected length, resembling “beads on a string” (discussed in §4). As we show in Fig. 4, a histogram of pro-

¹¹ <http://www.stsci.edu/~dcoe/trilogy/>

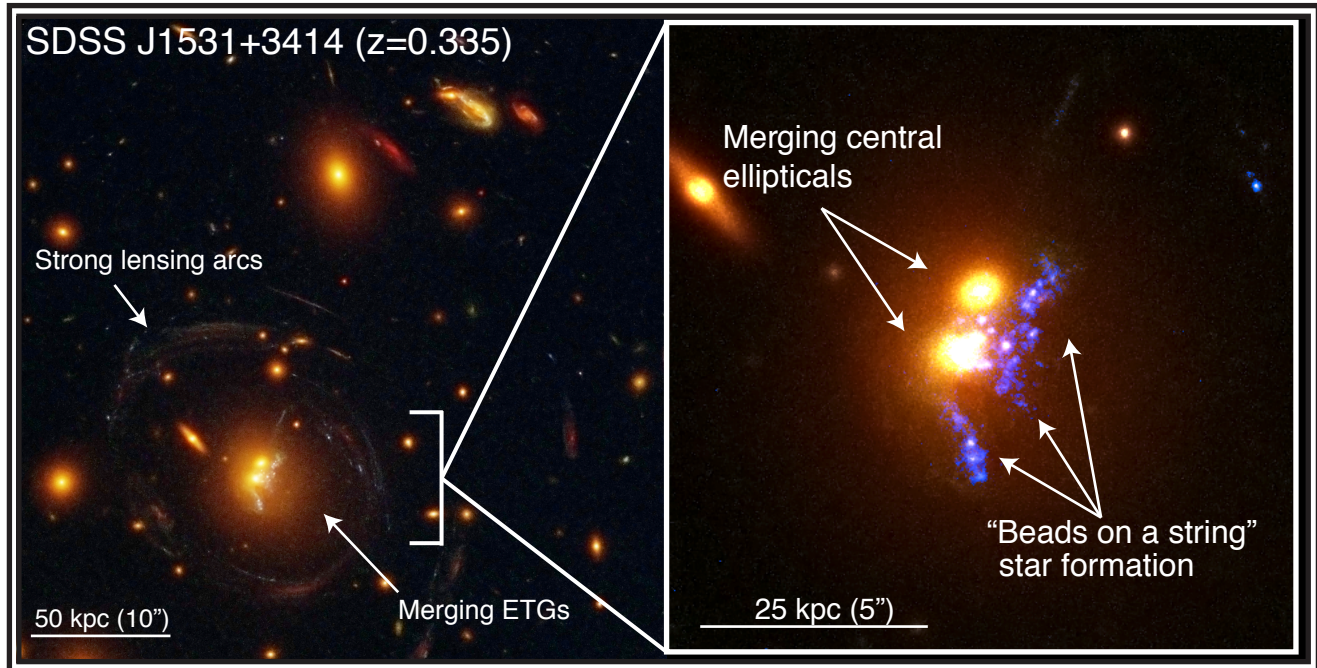


FIG. 1.— A four-color composite *HST*/WFC3 image of the strong lensing cluster SDSS J1531+3414 and its two central brightest cluster galaxies that are likely undergoing a major merger. The F160W and F814W images are shown in yellow/orange, the F606W image is shown in green, and the F390W image containing rest-frame near-ultraviolet emission from young stars is assigned to the blue channel. (*left*) A wide ($\sim 200 \times 200$ kpc²) view of the galaxy cluster. Tangential gravitational arcs from strongly lensed background galaxies are clearly seen. (*right*) A zoom-in on the left-hand panel, showing the two merging central cluster galaxies. Bright NUV emission associated with ongoing star formation is observed in blue.

jected separations between neighboring stellar clusters reveals a strong peak around $\sim 1-2$ kpc. All 19 clusters are at least marginally resolved, and while most are roughly circular, a few (especially cluster #2) show evidence for ~ 500 pc-scale asymmetries reminiscent of tidal arms.

Two filamentary strings of clusters (containing clusters numbered 6–9 and 15–19 on the bottom-right panel of Fig. 2) are aligned along a position angle that is roughly parallel to the axis joining the nuclei of the two merging galaxies (P. A. $\sim -45^\circ$, measured North through East). The other two strings (containing clusters 1–4 and 11–14, excluding #13) lie along a P. A. $\approx 45^\circ$ that is roughly perpendicular to this axis. The clusters are entirely contained within the combined projected old stellar envelope of both galaxies, within a circle of diameter ~ 27 kpc ($5''.6$). This can be seen in the top-left panel of Fig. 2, in which the NUV continuum emission is plotted in green contours over the F160W image, showing the old stellar population.

4. DISCUSSION

4.1. Origin of the ultraviolet emission

We consider three scenarios for the physical nature and origin of the clumpy NUV continuum emission.

1. It is a gravitationally lensed image (or a set of images) from a higher redshift background galaxy (or multiple galaxies).
2. It is a chance superposition along the line of sight, arising instead from a projection effect due to unrelated foreground sources.
3. It arises from ongoing or very recent star formation taking place within the stellar envelope of the interacting elliptical galaxies.

Scenarios (1) and (2) are entirely ruled out by spectroscopic evidence. The same SDSS and NOT spectroscopy used to confirm that the two elliptical galaxies are indeed merging also confirms that $H\alpha$ and $[O\ II]$ emission from star formation is mapped to the same redshift of the galaxies at $z = 0.3350 \pm 0.0002$ (see Fig. 3). The stellar superclusters therefore must inhabit the combined stellar envelope of the merger participants. The integrated flux density of the NUV continuum in the F390W bandpass is $(5.161 \pm 0.512) \times 10^{-17}$ erg sec⁻¹ cm⁻² Å⁻¹, suggesting that line emission from the young stellar superclusters is easily bright enough to be detected in the spectroscopy. If at appreciably different redshift than the two galaxies with which the emission is cospatial, the redshift of the Balmer lines should be offset from that of the Mg and Na D absorption as well as the calcium break. Moreover, strong lensing analysis (Sharon et al. 2014, submitted to ApJ) indicates that possible lensed images of background sources do not contribute significantly to the flux seen in the NUV emission. For the remainder of this Letter, we therefore adopt the most evidence-supported scenario (3), and conclude that (a) the two elliptical galaxies seen in close separation are indeed undergoing a major merger and (b) the clumpy NUV continuum emission arises from ongoing or recent star formation taking place within their combined stellar envelope.

4.2. Properties of the young stellar superclusters

The integrated SDSS $H\alpha$ line flux from the $3''$ diameter fiber, which covers only the innermost region of the star forming chain (see Fig. 3, top right), is $(6.335 \pm 1.77) \times 10^{-16}$ erg sec⁻¹ cm⁻² with a FWHM of 152 ± 15 km sec⁻¹. We estimate internal extinction via the Balmer decrement ($H\alpha/H\beta$ flux ratio), following the procedure described in Tremblay et al. (2010) and adopting “case B” recombination and the $R_V = 3.1$ reddening-to-extinction law of Cardelli et al. (1989). After an

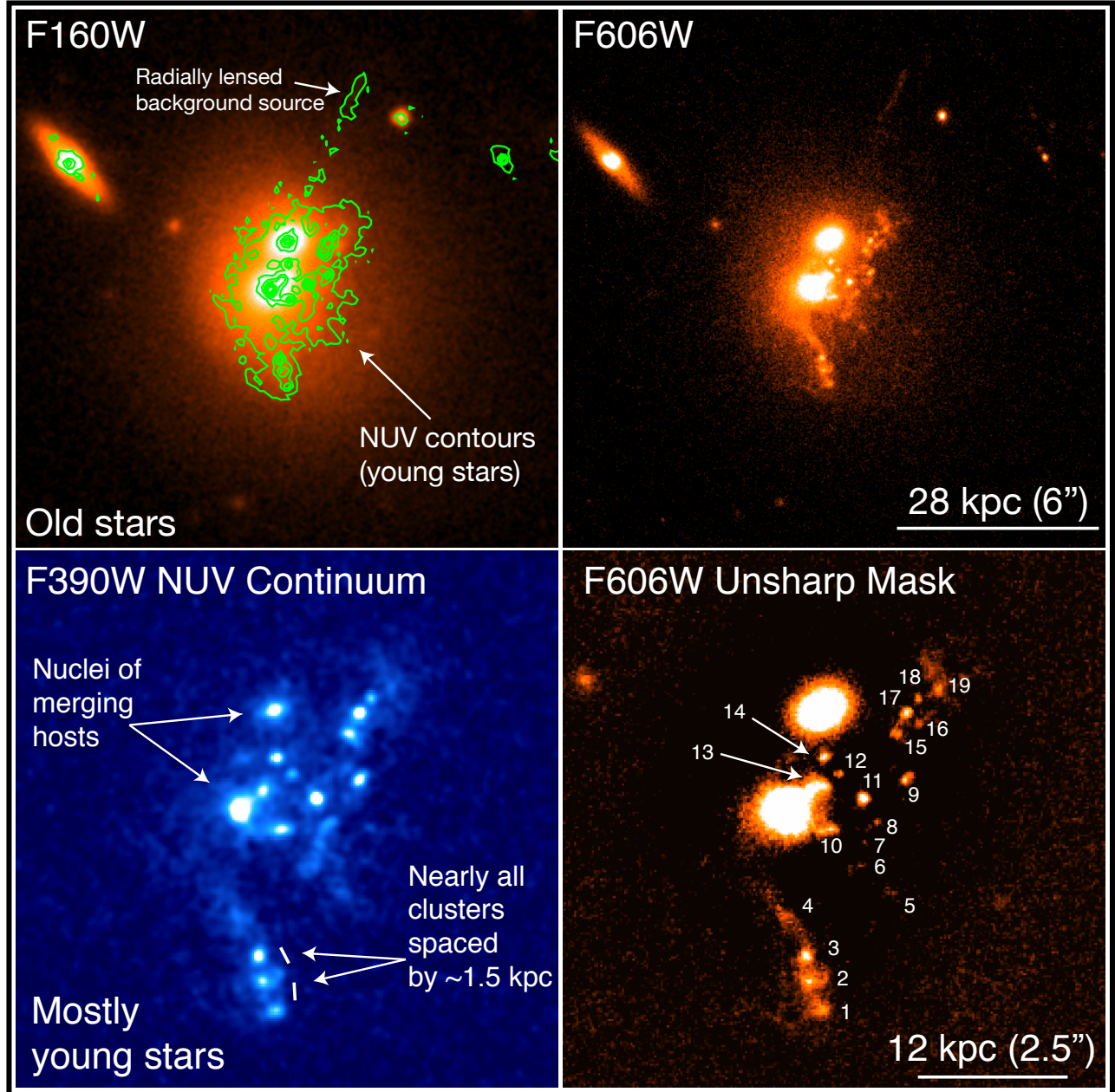


FIG. 2.— (*top left*) F160W image of the old stellar population associated with the two merging elliptical galaxies. NUV continuum emission (from the F390W image) is overlaid in green contours, marking the location of the young stars relative to the nuclei and old stellar envelopes of the merging host galaxies. The linear NUV feature marked with the arrow in this panel is a radial arc from a lensed background galaxy (Sharon et al. 2014, in prep). (*top right*) F606W image of both the old and young stellar component. (*bottom left*) F390W rest-frame NUV continuum image (zoomed-in slightly with respect to the top two panels). The image has been lightly smoothed with a gaussian kernel. The NUV emission arises mostly from young stars associated with ongoing or recent star formation. The nuclei of the two merging elliptical host galaxies are labeled with white arrows. (*bottom right*) Unsharp mask of the F606W image revealing residual fluctuations from the overall surface brightness profile, possibly due to [O II] and blue excess emission. The stellar superclusters to which we directly refer in the text are numerically labeled in this panel. The centroids of all panels are aligned, with East left and North up. The top row of images shows a slightly wider field of view than the bottom row.

additional correction for foreground Milky Way extinction using $E(B-V) = 0.023$, we estimate an extinction-corrected $H\alpha$ luminosity of $(3.65 \pm 1.1) \times 10^{41}$ erg sec^{-1} from the region covered by the SDSS fiber. As part of our NOT/ALFOSC observations, we used a $2''.5$ wide slit to observe the stellar superclusters in $H\alpha$, as detailed in Figure 3. This slit encompasses all of the NUV identified clumps, even after accounting for minimal slit losses given ground-based seeing. The derived $H\alpha$ line flux from our ALFOSC data is 1.7 times greater than that reported by SDSS, approximately as expected given

the more complete spatial coverage of the clumps by the wide slit observation. Including a 30% uncertainty to account for spectrograph CCD fringing and our [N II] contamination correction, the implied total extinction-corrected $H\alpha$ luminosity for the entire system is $(6.21 \pm 1.9) \times 10^{41}$ erg sec^{-1} .

By Eq. 2 in Kennicutt (1998), this extinction-corrected $H\alpha$ luminosity corresponds to a (very rough and assumption-heavy) star formation rate (SFR) of $\sim 5 \pm 2 M_{\odot} \text{ yr}^{-1}$. Automated modeling of the SDSS spectrophotometric data by Maraston et al. (2009, 2006, 2013), which matches SED tem-

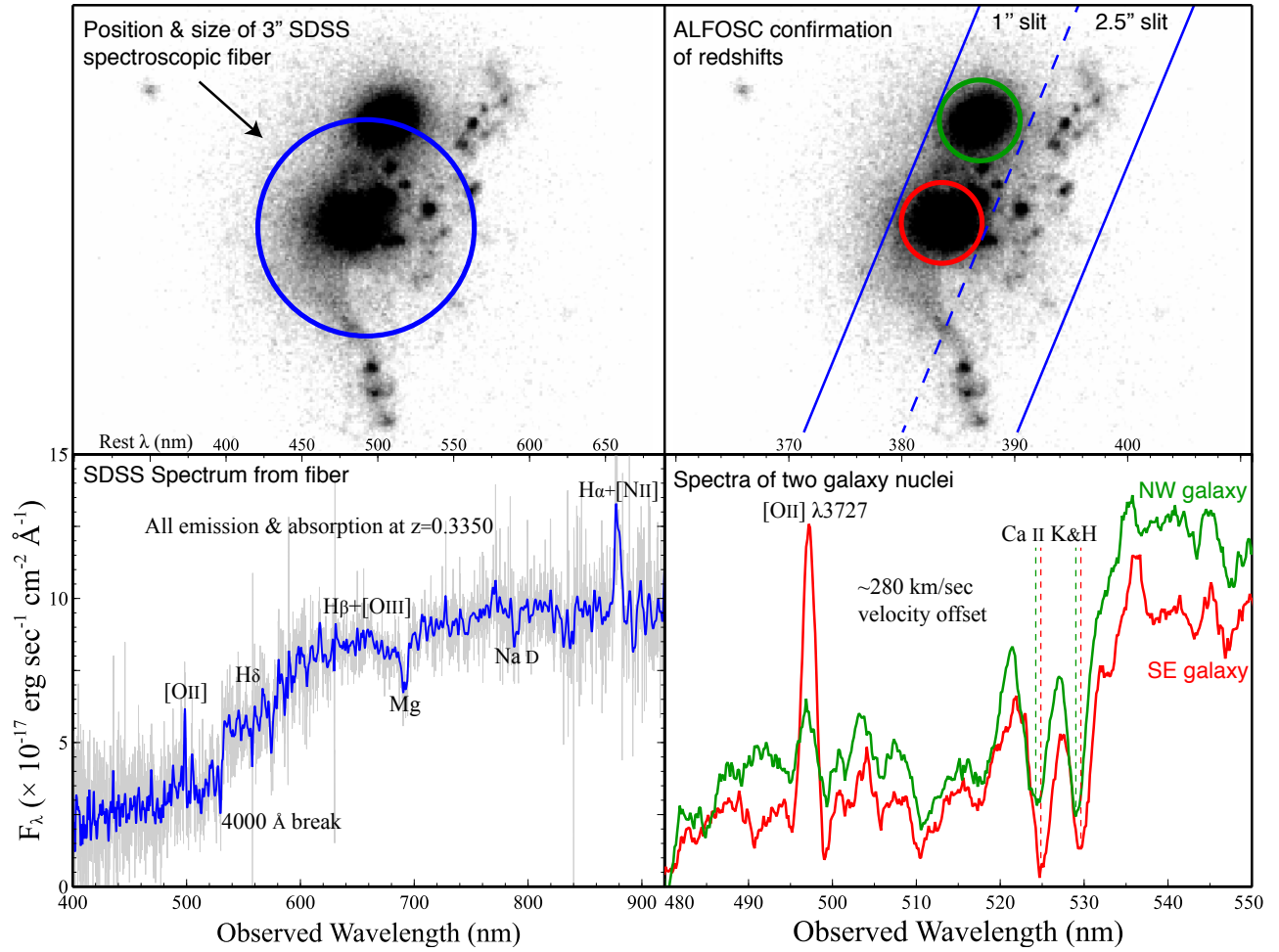


FIG. 3.— (*left panels*) SDSS optical spectrum of the central BCGs, coming from a $3''$ diameter spectral fiber whose position and relative size is marked by the blue circle on the *HST* F606W image at top left. All detected emission and absorption lines in the spectrum are at a uniform redshift of $z = 0.3350 \pm 0.0002$, including $H\alpha$ emission from the young stars and Mg+Na D absorption and 4000 Å break from the old stellar population in the galaxies. (*right panels*) Follow-up NOT/ALFOSC slit spectroscopy. Position and P. A. of the $1''$ and $2.5''$ spectroscopic slits are marked on the F606W image in the top right panel. The bottom right panel shows extracted spectra from the northwestern (NW) and southeastern (SE) halves of the $1''$ slit in green and red, respectively. Emission in both halves of the slit is dominated by the two elliptical galaxy nuclei. The galaxies are at the same redshift of $z = 0.335$, as can be seen by the close wavelength alignment of all spectroscopic features.

plates to extinction-corrected SDSS *ugriz* magnitudes, yields an SFR of $9.55 \pm 3.4 M_{\odot} \text{ yr}^{-1}$ and a total stellar mass of $(3.35 \pm 0.04) \times 10^{11} M_{\odot}$ (for more details, see Maraston et al. 2006). Absent the follow-up data needed for a more robust analysis, the remainder of this Letter assumes that the SFR is roughly in the range of $\sim 5 - 10 M_{\odot} \text{ yr}^{-1}$. Each clump contributes approximately $\sim 2 - 6\%$ of the total NUV flux, which should roughly scale to its relative contribution to the total star formation rate. We therefore estimate that the clumps have an associated star formation rate in the range of $\sim 0.1 - 0.6 M_{\odot} \text{ yr}^{-1}$.

Inverting the Bigiel et al. (2008) calibration of the molecular Schmidt law (Kennicutt 1998) and assuming gas depletion times in the range of 1–2 Gyr, the total SFR translates to a rough associated molecular gas mass of $M_{\text{H}_2} \approx 0.5 - 2 \times 10^{10} M_{\odot}$. We obtained an IRAM 30m telescope CO(1–0) observation in an attempt to measure the actual cold gas mass. No line was detected at a sensitivity of 0.9 mK T_{mb} per 80 km sec^{-1} channel, setting a 1σ upper limit of $\sim 1 \times 10^{10} M_{\odot}$ of molecular gas, assuming a line width of 220 km s^{-1} and a Galactic X_{CO} factor. A molecular gas mass in the range of

$\sim 0.5 - 1 \times 10^{10} M_{\odot}$ would be $\sim 1 - 3\%$ that of the galaxies’ stellar mass, consistent with that observed in large samples of early type galaxies (e.g., Young et al. 2011).

The observed star formation in SDSS 1531 is strongly reminiscent of the well-known “beads on a string” mode of star formation (e.g., Chandrasekhar & Fermi 1953; Toomre 1977; Elmegreen & Efremov 1996; Renaud et al. 2008) frequently observed in the arms of spiral galaxies (Elmegreen & Elmegreen 1983), resonance rings (Elmegreen 1994), and tidal arms that bridge interacting galaxies (Duc et al. 2000; Smith et al. 2010). Beads on a string star formation is a kpc-scale manifestation of the Jeans length, and the physics governing the system is analogous to the Plateau-Rayleigh instability causing (e.g.) a continuous column of falling water to disrupt, explaining why rain falls in drops rather than in unbroken filaments from the sky (e.g., Quillen & Comparella 2010). Despite being broadly categorized as “red and dead”, it has been known for a number of years that star formation can be relatively abundant in both cluster and field ellipticals (Yi et al. 2005; O’Dea et al. 2008; Jeong et al. 2009; Davis et al. 2011; Tremblay et al. 2012). Nevertheless, the formation of “beads on a string” stellar superclusters in major,

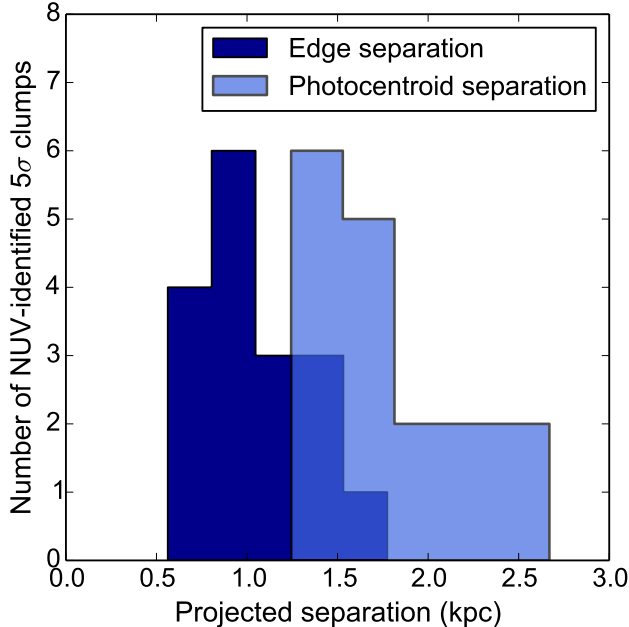


FIG. 4.— Projected separations, in kpc, between adjacent NUV-bright clumps associated with $\geq 5\sigma$ count rate overdensities in the *HST* F390W image. The light blue histogram shows measured separations between clump centroids, and the dark blue histogram shows separation between the edges of those adjacent clumps, where a clump edge is roughly defined as the radial boundary encompassing $\sim 90\%$ of all flux associated with the clump. Clump centroids are generally spaced ~ 1.5 kpc in projection from one another, whereas the projected separation between the edges of clumps is ~ 1 kpc. Typical resolved clump diameters are ~ 1 kpc. On galaxy-wide scales, the “beads on a string” mode of star formation is believed to be associated with the formation of Jeans length superclusters separated by 1–2 kpc from one another, consistent with what is observed here.

likely gas-rich mergers between giant ellipticals is rarely (if ever) observed, regardless of whether or not the star formation is driven by a merger or a cooling flow (e.g., Tremblay et al. 2014b, in prep). The unusual system in SDSS 1531 is likely a serendipitous snapshot of what may be a very short-lived morphology, presenting a unique opportunity to study star formation and gas dynamical response in a tidal field governed by dynamical friction, shear, and gravitational torques associated with the two merging ellipticals. Forthcoming cluster mass reconstruction from strong lensing (Sharon et al. 2014, submitted to ApJ.) will provide a well-constrained canvas against which these kinematics may be studied.

These quantitative analyses, however, await the necessary multiwavelength follow-up data. Recently obtained Gemini GMOS-N IFU observations (Tremblay et al. 2014c, in prep)

will disentangle the kinematics, dynamical timescales, and 3D geometry of the system, as well as local internal extinction corrections required for a better SFR estimate. ALMA is the only facility with the sensitivity and resolution needed to independently constrain the clump-by-clump SFR and molecular gas masses.

Finally, *Chandra* X-ray observations would determine whether or not the observed star formation might originate from gas that has condensed from the ambient hot atmosphere via a cooling flow, or a shock in the X-ray gas driven by colliding hot halos from the galaxy merger. The location of the stellar superclusters leaves this origin question open, as the star formation is not occurring in a region between the merging galaxies, where one would most obviously expect it if the star formation is shock triggered. However, viscous drag effects preferentially influencing the gas may be responsible for the apparent dislocation of the stellar (and presumably dark matter mass) components from the gas, as has been observed in other galaxy cluster mergers (e.g., Clowe et al. 2006).

We thank Profs. Françoise Combes, Eric Emsellem, and Tim de Zeeuw for thoughtful discussions. We also thank the anonymous referee whose feedback improved this work. G.R.T. and T.A.D. acknowledge support from a European Southern Observatory (ESO) Fellowship partially funded by the European Community’s Seventh Framework Programme (/FP7/2007-2013/) under grant agreement No. 229517. Support for program number HST-GO-13003 was provided by NASA through a grant from the Space Telescope Science Institute, which is operated by the Association of Universities for Research in Astronomy, Inc., under NASA contract NAS5-26555. This paper is based on observations by the NASA/ESA *Hubble Space Telescope*, obtained at the Space Telescope Science Institute. We also present results from the the Nordic Optical Telescope, operated by the Nordic Optical Telescope Scientific Association at the Observatorio del Roque de los Muchachos, La Palma, Spain, of the Instituto de Astrofísica de Canarias. Funding for the SDSS and SDSS-II has been provided by the Alfred P. Sloan Foundation, the Participating Institutions, the National Science Foundation, the U.S. Department of Energy, the National Aeronautics and Space Administration, the Japanese Monbukagakusho, the Max Planck Society, and the Higher Education Funding Council for England. The SDSS Web Site is <http://www.sdss.org/>.

REFERENCES

- Bayliss, M. B., Hennawi, J. F., Gladders, M. D., et al. 2011, *ApJS*, 193, 8
 Bayliss, M. B., Rigby, J. R., Sharon, K., et al. 2013, *ArXiv e-prints*, arXiv:1310.6695
 Bigiel, F., Leroy, A., Walter, F., et al. 2008, *AJ*, 136, 2846
 Cardelli, J. A., Clayton, G. C., & Mathis, J. S. 1989, *ApJ*, 345, 245
 Chandrasekhar, S., & Fermi, E. 1953, *ApJ*, 118, 116
 Clowe, D., Schneider, P., Aragón-Salamanca, A., et al. 2006, *A&A*, 451, 395
 Coe, D., Umetsu, K., Zitrin, A., et al. 2012, *ApJ*, 757, 22
 Davis, T. A., Alatalo, K., Sarzi, M., et al. 2011, *MNRAS*, 417, 882
 Dressel, L. 2012, *Wide Field Camera 3 Instrument Handbook for Cycle 21 v. 5.0*
 Duc, P.-A., Brinks, E., Springel, V., et al. 2000, *AJ*, 120, 1238
 Elmegreen, B. G. 1994, *ApJ*, 425, L73
 Elmegreen, B. G., & Efremov, Y. N. 1996, *ApJ*, 466, 802
 Elmegreen, B. G., & Elmegreen, D. M. 1983, *MNRAS*, 203, 31
 Fruchter et al. 2010, in *2010 Space Telescope Science Institute Calibration Workshop*, p. 382-387, 382–387
 Gralla, M. B., Sharon, K., Gladders, M. D., et al. 2011, *ApJ*, 737, 74
 Hennawi, J. F., Gladders, M. D., Oguri, M., et al. 2008, *AJ*, 135, 664
 Jeong, H., Yi, S. K., Bureau, M., et al. 2009, *MNRAS*, 398, 2028
 Kaviraj, S., Darg, D., Lintott, C., Schawinski, K., & Silk, J. 2012, *MNRAS*, 419, 70
 Kennicutt, Jr., R. C. 1998, *ApJ*, 498, 541
 Maraston, C., Daddi, E., Renzini, A., et al. 2006, *ApJ*, 652, 85
 Maraston, C., Strömbäck, G., Thomas, D., Wake, D. A., & Nichol, R. C. 2009, *MNRAS*, 394, L107
 Maraston, C., Pforr, J., Henriques, B. M., et al. 2013, *MNRAS*, 435, 2764
 O’Dea, C. P., Baum, S. A., Privon, G., et al. 2008, *ApJ*, 681, 1035
 Oguri, M., Bayliss, M. B., Dahle, H., et al. 2012, *MNRAS*, 420, 3213
 Oguri, M., Hennawi, J. F., Gladders, M. D., et al. 2009, *ApJ*, 699, 1038

- Postman, M., Coe, D., Benítez, N., et al. 2012, *ApJS*, 199, 25
- Quillen, A. C., & Comparetta, J. 2010, ArXiv e-prints, arXiv:1002.4870
- Renaud, F., Boily, C. M., Fleck, J.-J., Naab, T., & Theis, C. 2008, *MNRAS*, 391, L98
- Smith, G. P., Khosroshahi, H. G., Dariush, A., et al. 2010, *MNRAS*, 409, 169
- Toomre, A. 1977, in *Evolution of Galaxies and Stellar Populations*, ed. B. M. Tinsley & R. B. G. Larson, D. Campbell, 401
- Tremblay, G. R., O’Dea, C. P., Baum, S. A., et al. 2010, *ApJ*, 715, 172
- . 2012, *MNRAS*, 424, 1042
- Yi, S. K., Yoon, S.-J., Kaviraj, S., et al. 2005, *ApJ*, 619, L111
- York, D. G., Adelman, J., Anderson, Jr., J. E., et al. 2000, *AJ*, 120, 1579
- Young, L. M., Bureau, M., Davis, T. A., et al. 2011, *MNRAS*, 414, 940